Determination of Isothermal Transformation Diagrams for Sigma-Phase Formation in Cast Duplex Stainless Steels CD3MN and CD3MWCuN

YOON-JUN KIM, L. SCOTT CHUMBLEY, and BRIAN GLEESON

Work was undertaken to establish reliable time-temperature-transformation (TTT) diagrams for the cast duplex stainless steels CD3MN and CD3MWCuN. The latter contains higher Cr, Ni, and Mo contents compared to the former. The TTT diagrams for sigma-phase formation in both alloys were developed based on quantitative metallography results from optical and scanning electron microscopy. The kinetics of sigma-phase were found to be much faster in CD3MWCuN alloys than in CD3MN. An Avrami analysis was employed to assess transformation characteristics and to refine the TTT diagram determination. Theoretical prediction of phase equilibria using the thermodynamic software package ThermoCalc was compared to the amount of sigma phase observed experimentally from long-term heat treatments. The constructed TTT diagrams of the cast alloys were compared to wrought counterpart alloys.

I. INTRODUCTION

DUPLEX stainless steels (DSSs) constitute a group of steels possessing both ferrite and austenite as the primary phases. The austenite + ferrite phase assemblage is attainable by combining various phase-stabilizing elements.[1,2,3] Both Cr and Mo are effective ferrite stabilizers, producing a wide ferrite phase field in temperature/steel-composition space. In general, stainless steels having ferrite as the predominant phase have excellent corrosion resistance due to the high solubility of Mo and Cr in ferrite. On the other hand, Ni and N, which are effective austenite stabilizers, increase the austenite phase field in Fe-based systems and are known to improve mechanical properties. Thus, a DSS containing relatively high and balanced Cr, Mo, Ni, and N contents has a favorable combination of mechanical properties and high corrosion resistance. The effect produced by these alloying elements on corrosion resistance is indicated by the pitting resistance equivalent number (PREN) given in Eq. [1].[4] In general, the higher the PREN the better the resistance of a DSS to localized corrosion. A duplex alloy having a PREN greater than 40 is categorized as a super duplex stainless steel (SDSS).

$$\text{PREN} = \text{wt pct Cr} + 3.3 \times \text{wt pct Mo} + 17 \times \text{wt pct N} \quad [1]$$

Duplex stainless steels have primary (δ and γ_1) and secondary (*e.g.*, γ_2, σ, χ, π, carbides, and nitrides) phases. Information on the reported phases in DSS is summarized in Table I. Previous studies[1–4] have shown that secondary phases in the form of intermetallics are detrimental to the mechanical and corrosion properties of the steels. Sigma is considered to be the most detrimental due to its potential to form a significant amount (up to about 30 vol pct)[1] in DSS. Therefore, knowledge of the kinetics of sigma-phase formation is important in order to control corrosion and mechanical properties.

YOON-JUN KIM, Graduate Student, and L. SCOTT CHUMBLEY and BRIAN GLEESON, Professors, are with the Department of Materials Science and Engineering, Iowa State University, Ames, IA 50011. Contact e-mail: yoonjun@iastate.edu

Manuscript submitted February 6, 2004.

A considerable number of studies has reported on the phase transformation behavior and associated effects of alloying elements, corrosion resistance, and mechanical properties of wrought DSS.[1–4,9–24] The effects of alloying elements on the formation of secondary phases are summarized in Figure 1.[1,4] However, even though cast DSSs are used in many applications, they have been the subject of little research. It should be expected that the phase transformation kinetics and even phase equilibria are different between the cast and wrought alloys due to differences in their nominal compositions as well as their microstructure. The aim of this article is to develop time-temperature-transformation (TTT, also known as isothermal transformation or IT) diagrams for two types of cast DSS alloys, designated CD3MN and CD3MWCuN, and to assess the observed phase transformation kinetics and characteristics.

II. EXPERIMENTAL PROCEDURES

A. *Materials*

Three different heats of CD3MN alloy were received from two different foundries and were denoted as $4A_1$, $4A_2$, and $4A_3$. Two heats of CD3MWCuN alloy were supplied from a single foundry and were denoted as $6A_1$ and $6A_2$. Although the suppliers and batches were different, the alloy compositions were quite similar, as shown in Table II. Samples were provided in the form of keel bars of approximate dimensions $3 \times 4 \times 35$ cm. Small coupons about 4-mm thick were sliced from sections of the bars by electrical discharge machining (EDM). A 3-mm-diameter hole was drilled at the top of each coupon in order to attach a wire for suspending the coupons inside the vertical furnace and salt bath. For long-time heat treatments, some samples were encapsulated in quartz tubes filled with Ar gas in order to reduce the extent of oxidation. Encapsulated samples were somewhat smaller, having EDM prepared dimensions of about $4 \times 8 \times 25$ mm.

While all alloys were received in a heat-treated state, they were reheated to 1100 °C, at which the ratio of ferrite to austenite is predicted to be 50:50 vol pct. This reheating was done for 30 minutes, with the assumption being that the

Table I. General Information on Common Secondary Phases in DSSs[2]

Phase	Lattice Type (Structure Type)	Space Group	Lattice Parameter, Å	Formation Temperature, °C	Properties
δ	bcc (W)	$Im\bar{3}m$	a = 2.86 to 2.88	all temperatures	good corrosion resistance
γ/γ_2	fcc (Cu)	$Fm\bar{3}m$	a = 3.58 to 3.62	700 to 900 (γ_2)	good mechanical properties, γ_2 may have eutectic morphology
σ	tetragonal (CrFe)	$P4_2/mnm$	a = 8.79, c = 4.54	600 to 1000	detrimental for mechanical properties and corrosion
χ	cubic (Mn)	$I\bar{4}m$	a = 8.92	700 to 900	similar to sigma, but higher Mo content (≈20 wt pct)
R	rhombohedral (Mo)	$R3$	a = 10.90, c = 19.34	550 to 800	Mo rich (≈40 wt pct maximum) phase, detrimental
π	cubic (Mn)	$P4_132$	a = 6.47	≈600	detrimental to toughness and pitting corrosion resistance
Cr_2N	hexagonal (Fe-N)	$P\bar{3}1m$	a = 4.80, c = 4.47	700 to 900	detrimental to corrosion resistance
$M_{23}C_6$	cubic (C_6Cr_{23})	$Fm\bar{3}m$	a = 10.56 to 10.65	<950	less important than other phases due to low carbon content
M_7C_3	orthorhombic (C_3Cr_7)	$Pnma$	a = 4.52, b = 6.99, c = 12.11	950 to 1050	in DSS or super DSS

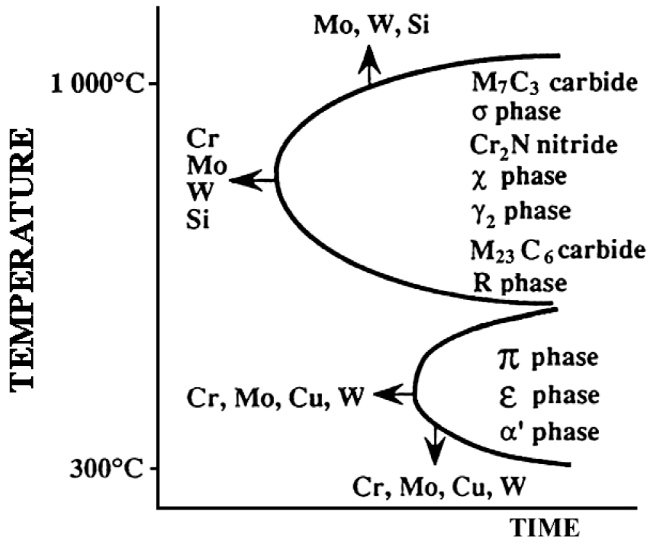

Fig. 1—Secondary phases in DSSs and the effects of alloying elements on the location and shape of the TTT curve for these phases.[2,5]

foundry heat treatment was sufficient to dissolve and homogenize the structure, Table I such that this latter treatment was simply to produce a common starting ferrite/austenite ratio for a given alloy.

B. *Heat Treatment*

The transformation kinetics and phase constituents that resulted due to quenching followed by isothermal holds were examined and directly measured by quantitative analysis using standard metallographic techniques. The experimental details have been described previously.[5] Briefly, samples were heat treated in the temperature range 700 °C to 900 °C for times ranging from 1 minute to 30 days. Short-term treatments were done using a salt pot, while long-term heat treatments were performed using box furnaces. Table III summarizes the heat-treatment schedules.

The center regions of the heat-treated samples were examined in order to avoid any surface effects. Metallographic cross sections were prepared using standard techniques. The polished samples were electrolytically etched in a sodium hydroxide solution (50 g NaOH to 100 mL H_2O) or potassium hydroxide solution (50 g KOH to 100 mL H_2O) at 6 V for 10 seconds. This electrolytic etching tints the ferrite a light blue and the sigma a reddish brown.[3,5]

An image analysis system was used to measure the amount of sigma (*i.e.*, assumed area fraction = volume fraction) in the cross-sectional images. Ten randomly selected areas were taken at 200 times magnification for image analysis of a given sample. The etch technique used tints the sigma and chi phases the same color. Therefore, the measured amount of sigma phase is more properly the amount of $\sigma + \chi$. For the purposes of presentation in this study, the term σ should properly be considered a mixture of σ plus small amounts of χ, as will be discussed in Section IV–D.

A JEOL* 5910LV scanning electron microscope (SEM) equipped with an energy-dispersive X-ray spectrometer (EDS) was used for additional microstructural observations.

*JEOL is a trademark of Japan Electron Optics Ltd., Tokyo.

C. *Avrami Analysis*

The extent of sigma formation as a function of isothermal hold time can be described using the Avrami equation.[6] The general form of this equation is

$$f = \frac{V}{V_e} = 1 - \exp(-kt^n) \qquad [2]$$

where f is the fraction transformed, k is a reaction constant in min^{-n}, and the exponent n is a dimensionless constant that depends on the combination of nucleation and growth mechanisms for the transformation in question. In order to obtain the transformed volume fraction (f), it is necessary to find the equilibrium volume percent (V_e) at the temperature of interest. Extremely long-time anneals (30 days) were therefore done to determine V_e. The data were then fit to

Table II. ASTM Standard and Measured Compositions in Weight Percent of the Steels Used in This Study

Element	ASTM (CD3MN)	$4A_1$	$4A_2$	$4A_3$	ASTM (CD3MWCuN)	$6A_1$	$6A_2$
C	0.03_{max}	0.026	0.029	0.026	0.03_{max}	0.034	0.028
Mn	1.50_{max}	0.81	0.60	0.47	1.00_{max}	0.59	0.80
Si	1.00_{max}	0.66	0.65	0.57	1.00_{max}	0.87	0.75
P	0.04_{max}	0.014	0.025	0.024	0.03_{max}	0.023	0.03
S	0.020_{max}	0.0065	0.022	0.002	0.025_{max}	0.011	0.011
Cr	21.0 to 23.5	22.10	22.12	22.00	24.0 to 26.0	24.53	24.68
Ni	4.5 to 6.5	5.44	5.45	5.50	6.5 to 8.5	7.33	7.38
Mo	2.5 to 3.5	2.91	2.98	2.82	3.0 to 4.0	3.62	3.54
Cu	1.00_{max}	0.152	0.225	0.194	0.5 to 1.0	0.668	0.918
W	—	—	0.063	0.059	0.5 to 1.0	0.757	0.752
N	0.10 to 0.30	0.17	0.15	0.14	0.20 to 0.30	0.23	0.29
Fe	bal	bal	bal	bal	bal	bal	bal

Table III. Heat-Treatment Schedule for the Different Batches of Alloys Used in This Study

(a) CD3MN

	Time, minutes													
Temp., °C	1	10	30	60	120	300	480	720	1440	2880	4320	7200	18720	43200
700	■	■	■	■	■	■	▲	▲	▲	▲	●	▲	▲	▲
750	■	■	■	■	■	■	▲	▲	▲	▲	●	▲	▲	▲
800	■	■	■	■	■	■	▲	▲	▲	▲	●	▲	▲	▲
850	■	■	■	■	■	■	▲	▲	▲	▲	●	●	●	●
900	■	■	■	■	■	■	■	■	■	■	●	▲	▲	▲

●$4A_1$ ■$4A_2$ ▲$4A_3$

b) CD3MWCuN

	Time, minutes							
Temp., °C	1	3	10	30	45	60	100	4320
700	●	●	●	●	■	■	●	●
750	●	●	●	●	■	■	●	●
800	●	●	●	●	■	■	●	●
850	●	●	●	●	■	■	●	●
900	●	●	●	●	■	■	●	●

●$6A_1$ ■$6A_2$

Eq. [2], with the n and k in this equation determined on the basis of the following equations:

$$n = \frac{\ln \frac{\ln (1 - V_1/V_e)}{\ln (1 - V_2/V_e)}}{\ln t_1/t_2} \quad [3]$$

$$k = \frac{-\ln (1 - V_1/V_e)}{t_1^n} \quad [4]$$

where t_1 and t_2 are isothermal hold times 1 and 2, respectively, and V_1, V_2, and V_e are volumes for times t_1, t_2, and equilibrium, respectively.

III. RESULTS

A. *TTT Diagram for CD3MN*

Metallographic examination of CD3MN samples showed that carbides can form at high temperatures and short soak times, while secondary austenite (γ_2) forms sympathetically at the primary austenite (γ_1/ferrite boundaries.[5] It was further shown that sigma forms at the γ_2/ferrite boundaries in the temperature range 700 °C to 900 °C. Both γ_2 and the sigma precipitates grew into the ferrite matrix. Typical micrographs of CD3MN are shown in Figure 2.

Figure 3 shows the measured volume percent of sigma in CD3MN as a function of isothermal annealing time in the temperature range 700 °C to 900 °C, with the corresponding data summarized in Table IV. It is seen in Figure 3 that the extent of sigma formation as a function of time follows the usual sigmoidal behavior in accordance with Eq. [2]. Table V lists the equilibrium volume percentages and the calculated n and k values for the various soak temperatures. The corresponding Avrami curves are shown in Figure 4. The times separating the limits in a given Avrami curve, *i.e.*, $f \approx 0$ and $f \approx 1$ represent the start and finish times for the transformation. For the curves shown in Figure 4, sigma formation was fastest at 850 °C and slowest at 700 °C. The calculated n values in Table V range from 1.4 to 2.6, indicating that the sigma formation is diffusion controlled, with the sigma precipitates forming at a small nucleation rate and growing from small dimensions.[6]

The Avrami equations that were determined were further used to establish TTT curves for 1, 50, and 99 pct sigma transformation. The results are shown in Figure 5. Conventionally, the initial curve is representative of 1 pct transformation and the final curve is regarded as 99 pct completed. The nose of the initial curve is located in the temperature range 800 °C and 850 °C at a time of about 70 minutes.

B. *TTT Diagram for CD3MWCuN*

Cross-sectional micrographs of the CD3MWCuN steel after different heat treatments are shown in Figure 6. Sigma

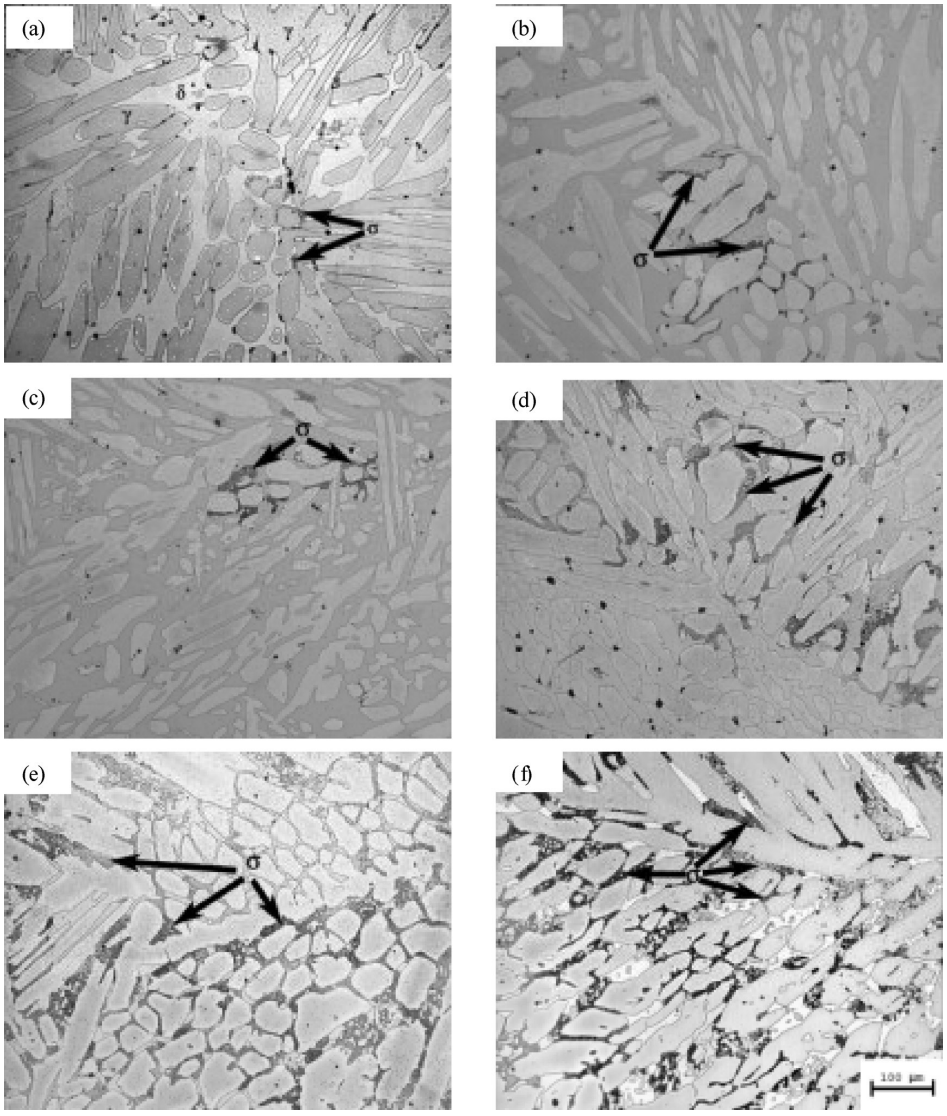

Fig. 2—Optical micrographs of the CD3MN after soaking for (*a*) 5, (*b*) 8, (*c*) 24, and (*d*) 48 h, and (*e*) 13 and (*f*) 30 days at 900 °C.

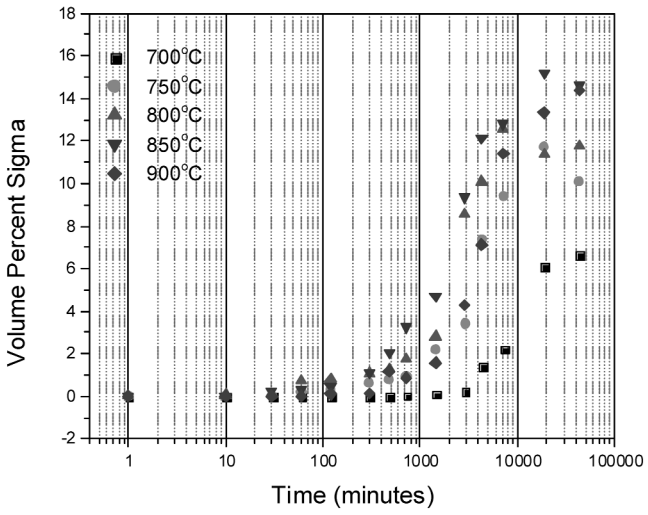

Fig. 3—The volume percent of sigma measured in CD3MN as a function of soak time at various temperatures.

formation in CD3MWCuN initially occurred at ferrite/austenite grain boundary and grew much more rapidly and extensively than in CD3MN, ultimately appearing eutectoid-like in structure at long aging time (Figure 6(f)). According to SEM/EDS analysis and color tint etching, this morphology appears to be a consequence of the ferrite matrix decomposing to secondary austenite and sigma. Figure 7 shows the amount of sigma formed as a function of isothermal hold time and temperature.

Avrami analyses for CD3MWCuN were carried out in the same manner as for CD3MN. As shown in Table VI and Figure 7, the equilibrium amount of sigma formed within only 3 days in comparison to 30 days for CD3MN. The results from the Avrami calculations for CD3MWCuN are listed in Table VII, and the corresponding Avrami curves are shown in Figure 8. Calculated n values range from 2.7 to 3, indicating diffusion-controlled sigma formation, as found for CD3MN; however, the n values for CD3MWCuN further suggest that sigma formation takes place with precipitates forming at constant or increasing nucleation rates and growing from small dimensions.[6]

Table IV. Volume Percent (or Area Percent) Sigma Phase in CD3MN for Soak Time and Temperature

Time, min	700 °C	750 °C	800 °C	850 °C	900 °C
1	0 ± 0	0 ± 0	0 ± 0	0 ± 0	0 ± 0
10	0 ± 0	0 ± 0	0.07 ± 0.12	0 ± 0	0 ± 0
30	0 ± 0	0.02 ± 0.06	0.11 ± 0.13	0.26 ± 0.37	0.02 ± 0.05
60	0 ± 0	0.21 ± 0.44	0.71 ± 0.61	0.32 ± 0.19	0.01 ± 0.04
120	0 ± 0	0.30 ± 0.24	0.82 ± 0.50	0.50 ± 0.34	0.10 ± 0.09
300	0.03 ± 0.10	0.63 ± 0.49	1.08 ± 0.34	1.13 ± 0.44	0.13 ± 0.14
480	0.03 ± 0.03	0.77 ± 0.27	1.30 ± 0.19	2.07 ± 0.36	1.19 ± 0.97
720	0.04 ± 0.13	0.94 ± 0.51	1.73 ± 0.30	3.25 ± 1.24	0.87 ± 0.54
1440	0.14 ± 0.19	2.19 ± 0.30	2.79 ± 0.40	4.72 ± 1.98	1.57 ± 1.26
2880	0.25 ± 0.22	3.42 ± 1.16	8.54 ± 2.47	9.36 ± 2.46	4.28 ± 1.79
4320	1.43 ± 1.32	7.38 ± 0.83	10.09 ± 2.67	12.12 ± 3.63	7.13 ± 2.01
7200	2.24 ± 0.57	9.43 ± 2.35	12.58 ± 1.94	12.80 ± 1.61	11.42 ± 1.86
18720	6.13 ± 2.31	11.72 ± 2.54	11.37 ± 1.73	15.21 ± 2.92	13.33 ± 2.68
43200	6.64 ± 0.63	10.08 ± 0.88	11.75 ± 2.68	14.60 ± 2.77	14.39 ± 2.86

Table V. Avrami Analysis Results for the CD3MN Alloy

Temperature, °C	V_e, Pct	k, min^{-1}	n
700	~6.7	4.3×10^{-11}	2.6
750	~10.0	3.5×10^{-6}	1.5
800	~11.5	6.3×10^{-6}	1.5
850	~14.0	2.0×10^{-5}	1.4
900	~15.0	7.8×10^{-6}	1.4

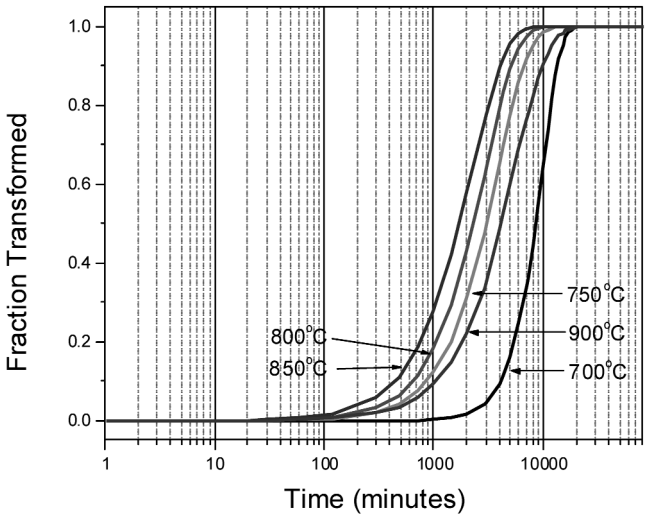

Fig. 4—Avrami curves determined for CD3MN.

Figure 9 shows a TTT diagram for CD3MWCuN that was constructed using the Avrami equations determined in this study. As done for CD3MN, TTT curves for 1 pct (initial), 50 pct, and 99 pct (final) sigma transformation are plotted. The nose of the initial curve is located between around 850 °C and 900 °C in as short as 5 minutes.

IV. DISCUSSION

A. *Avrami Analyses*

The TTT curves established in this study show that sigma formation is much more rapid in CD3MWCuN than in CD3MN, with equilibrium amounts of sigma in the former also being much higher. This may be expected, since sigma formation is related to the concentration of Cr and Mo in the steel, both of which are present in greater amounts in CD3MWCuN. Therefore, higher concentrations of those elements would be expected to increase the driving force for sigma nucleation. This indeed is reflected in the calculated n values from the Avrami analysis for both CD3MN and CD3MWCuN, which imply different phase transformation behaviors, particularly nucleation rates.

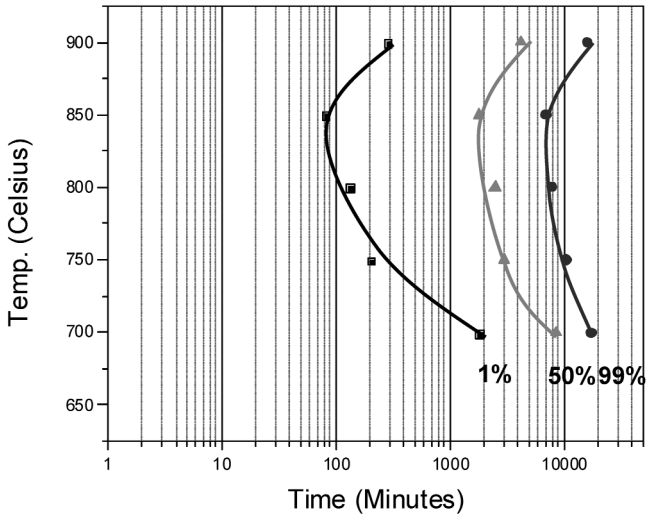

Fig. 5—Calculated TTT diagram of CD3MN.

The microstructures that developed in the two alloys upon formation of the sigma phase differed substantially from one another, being discrete precipitates in CD3MN and large regions of a eutectoid-like structure consisting of sigma and secondary austenite in CD3MWCuN. Associated with this morphology difference was the fact that the sigma formed at different rates and by different mechanisms in the two alloys, as indicated by the different exponent n values in the Avrami equation. The high n value (≈2.7 to 3) for CD3MWCuN indicates increasing nucleation and rapid growth. This would be consistent with a rapid structure formation as one expects to see in the closely spaced $\sigma + \gamma_2$ assemblage that developed in this alloy. Similarly, the lower n value for CD3MN (≈1.4 to 2.6) is consistent with

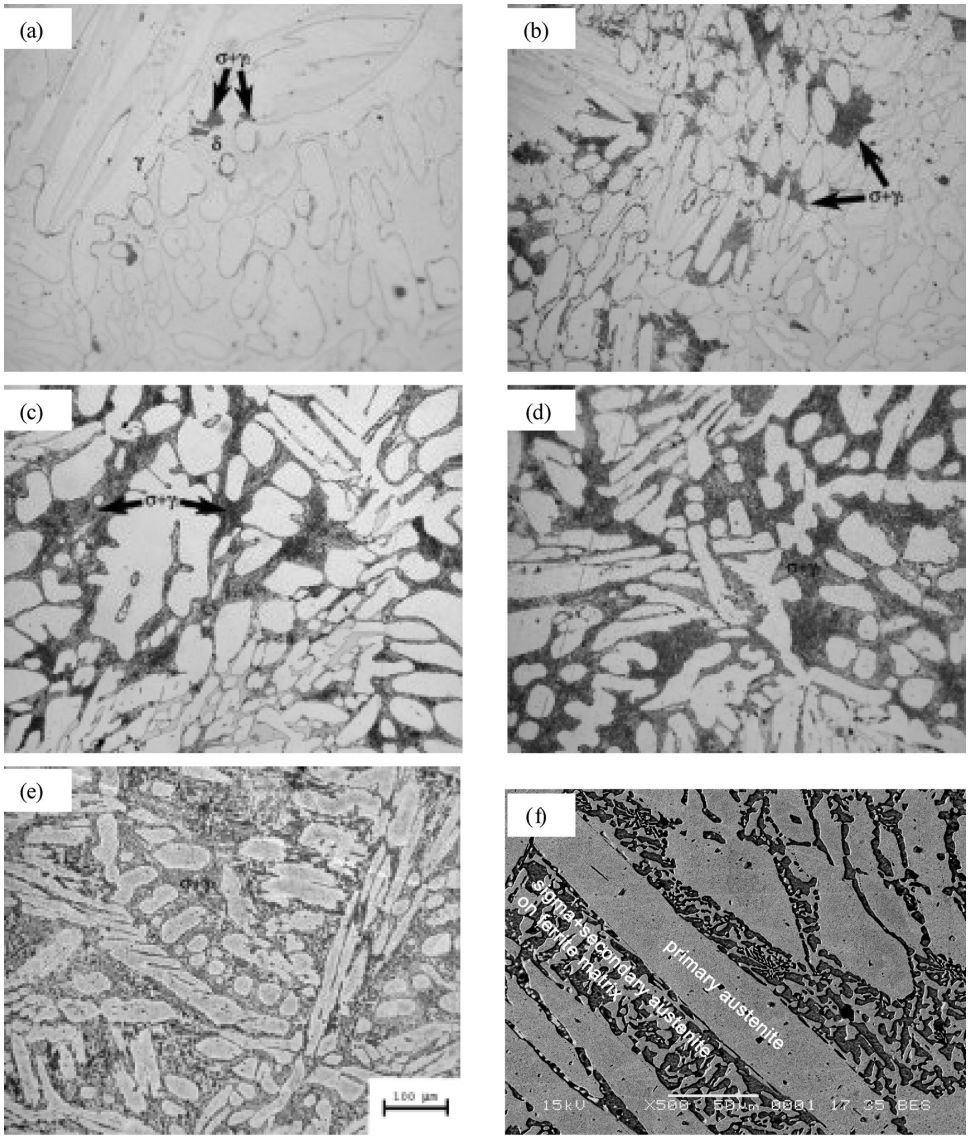

Fig. 6—Optical micrographs of CD3MWCuN after soaking for (*a*) 10, (*b*) 30, (*c*) 60, (*d*) 100, and (*e*) 4320 min at 900 °C and (*f*) SEM backscattered image after soaking for 4320 min at 900 °C.

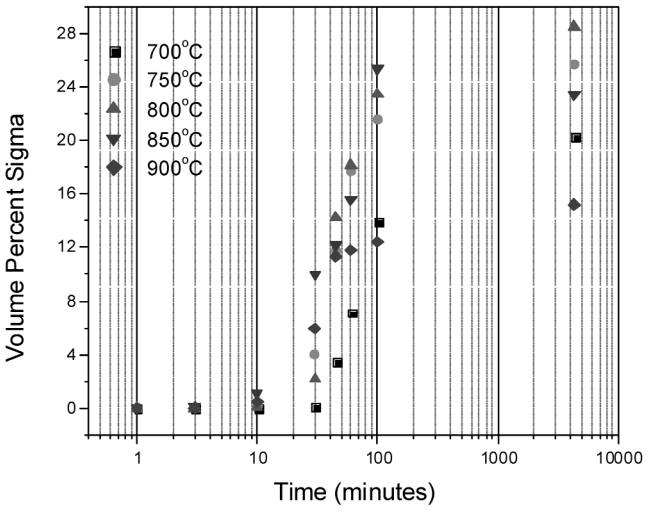

Fig. 7—The volume percent of sigma for measured in CD3MWCuN as a function of soak time at various temperatures.

precipitation and slow growth, as would be expected for the relatively isolated sigma precipitates in this alloy.

A more detailed analysis relating the rate of sigma formation to resulting growth morphology was not the goal of this particular study. In CD3MN alloys, it was noted that sigma nucleated preferentially at the ferrite and austenite grain boundaries and grew into the adjacent ferrite grains, as shown in Figures 2(a) and (b). It is also seen from Figures 2(a) through (e) that the size of sigma phase increased with increasing soak time as did the number density, although to a lesser extent. The final size of sigma phase shown in Figure 2(e) or (f) appeared obviously coarser with irregular shape than that of the early stage of heat treatment. In CD3MWCuN alloys, as mentioned, sigma started to nucleate at the ferrite/austenite interfaces, as shown in Figure 6(a), but a $\sigma + \gamma_2$ dual-phase morphology (*e.g.*, Figure 6(f)) was observed with an increase in soak time (Figures 6(b) through (e)). These observations agree with more detailed studies involving wrought alloy compositions, for which growth morphology and diffusion mechanisms were considered.[13,25,26] Further investigation on the

Table VI. Volume Percent Sigma in CD3MWCuN for Soak Time at Various Temperatures

Time, min	700 °C	750 °C	800 °C	850 °C	900 °C
1	0 ± 0	0 ± 0	0 ± 0	0 ± 0	0 ± 0
3	0 ± 0	0 ± 0	0 ± 0	0.11 ± 0.11	0.02 ± 0.02
10	0 ± 0	0.12 ± 0.19	0.09 ± 0.22	1.09 ± 0.89	0.49 ± 0.27
30	0.18 ± 0.39	4.01 ± 2.74	2.20 ± 2.38	9.95 ± 5.71	5.96 ± 3.19
45	3.53 ± 1.20	11.77 ± 1.80	14.27 ± 3.64	12.16 ± 2.33	11.34 ± 3.09
60	7.20 ± 1.60	17.67 ± 2.67	18.17 ± 3.99	15.61 ± 5.33	11.81 ± 0.93
100	13.99 ± 2.22	21.54 ± 2.84	23.42 ± 6.26	25.36 ± 5.47	12.41 ± 2.17
4320	20.35 ± 1.70	25.72 ± 3.25	28.48 ± 2.88	23.42 ± 5.21	13.53 ± 1.15

Table VII. Avrami Analysis Results for the CD3MWCuN Alloy

Temperature, °C	V_e, *p*ct	*k*, min^{-1}	*n*
700	~20	1.6×10^{-6}	3
750	~24.5	1.8×10^{-5}	2.7
800	~27	2.2×10^{-5}	2.7
850	~28	3.0×10^{-5}	2.7
900	~13	4.8×10^{-5}	2.7

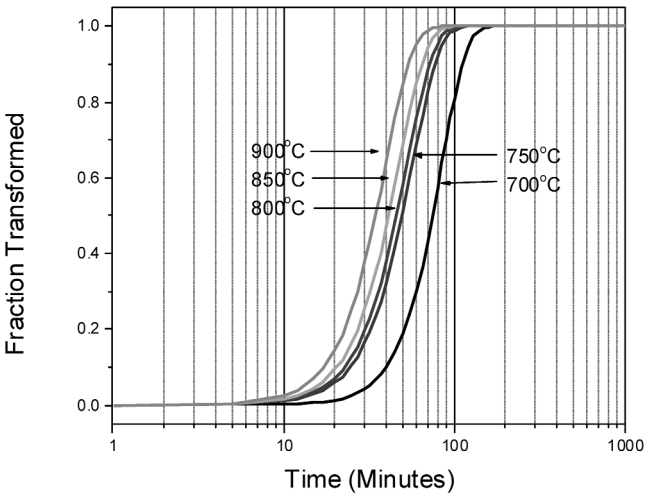

Fig. 8—Avrami curves determined for CD3MWCuN.

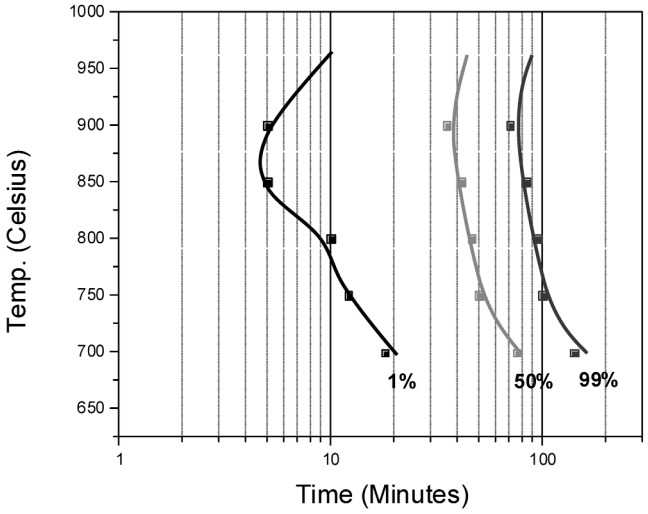

Fig. 9—Calculated TTT diagram of CD3MWCuN.

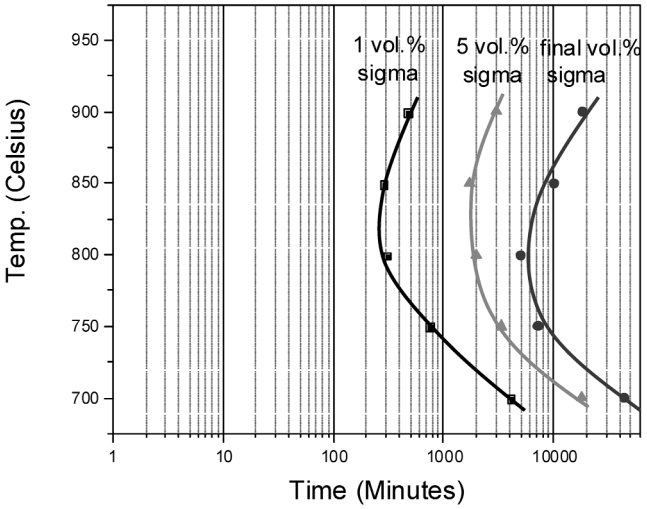

Fig. 10—Calculated precipitation curves of CD3MN.

microstructural evolution in the cast DSS alloys remains to be conducted with the aid of transmission electron microscopy.

B. *Relationship between Sigma Precipitate and Mechanical Property of DSS*

The TTT curves established in this study show that sigma formation is much more rapid in CD3MWCuN than in CD3MN, with equilibrium amounts of sigma in the former also being much higher. This may be expected, since sigma formation is related to the concentration of Cr and Mo in the steel, both of which are present in greater amounts in CD3MWCuN. It has been reported that sigma formation becomes detrimental to alloy toughness and corrosion resistance in DSSs when the amount present is greater than 5 vol pct.[1] The Avrami equations that were determined can be used to plot the times for the formation of an absolute volume percent of sigma (*i.e.*, rather than the percent transformation, as is done in Figures 5 and 9). Figures 10 and 11 show the TTT curves for 1, 5, and the final volume percent sigma in CD3MN and CD3MWCuN, respectively. It is seen from these figures that the times to reach 5 vol pct sigma formation are almost two orders of magnitude longer for CD3MN than for CD3MWCuN. Specifically, 5 vol pct sigma forms in CD3MWCuN in as short as 20 minutes at about 850 °C, while it takes a minimum of about 2000 minutes to form the same amount of sigma in CD3MN.[13, 25,26]

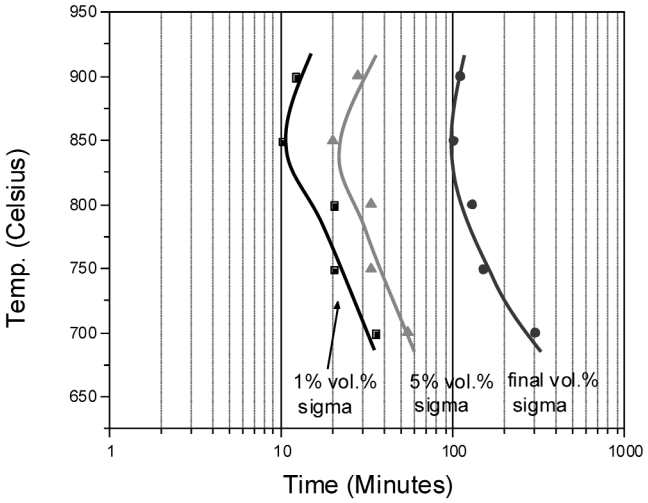

Fig. 11—Calculated precipitation curves of CD3MWCuN.

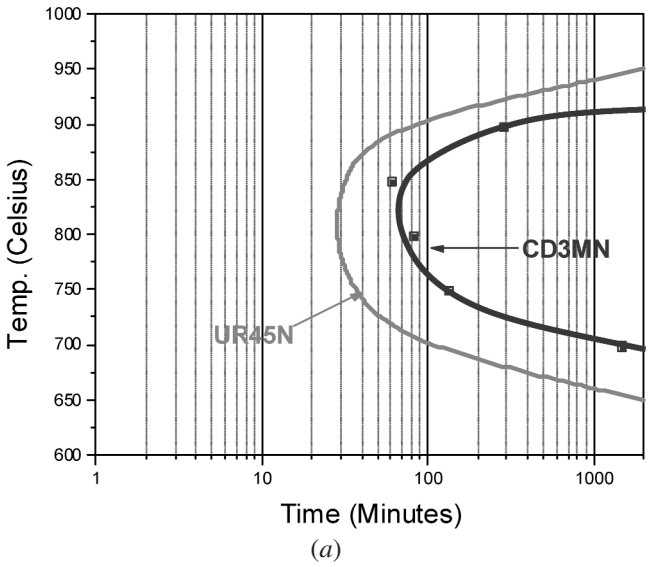

(*a*)

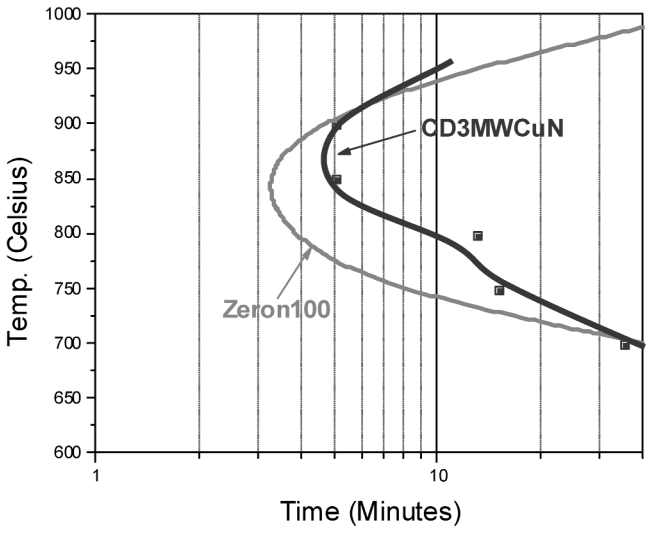

(*b*)

Fig. 12—Comparison to the TTT diagrams for (*a*) UR45N[3,5] and (*b*) Zeron 100[12] (wrought counterpart alloys for CD3MN and CD3MWCuN, respectively).

C. *Comparison to TTT Diagrams of Wrought Counterpart Alloys*

The TTT diagrams of several wrought DSS alloys have been published[2,4,13] and can be compared to the diagrams determined from this study. The alloy UR45N (alternatively designated by SAF 2205)* has a chemical composition similar to CD3MN, while Zeron 100* is somewhat comparable to CD3MWCuN. A comparison of the TTT diagrams (Figure 12) for the wrought *vs* the cast alloys shows that sigma formation starts at similar temperatures but at slightly delayed times in the cast alloys. As shown in Figure 12(a), for example, UR45N has the nose in the sigma curve at around 25 minutes and 850 °C compared to 60 minutes and 850 °C for CD3MN. Similarly, Zeron 100, shown in Figure 12(b), has the nose in the sigma curve at about 2.7 minutes and 850 °C compared to about 4.5 minutes and 850 °C for CD3MWCuN. These comparisons indicate that differences in microstructure between cast and wrought alloys may play a role in affecting the kinetics of sigma-phase formation. In terms of differences in microstructures, defects, *e.g.*, dislocations or grain boundaries, formed in wrought alloys during fabrication may effectively promote sigma formation.

*SAF 2205 is a trademark of Sandvik Steel, Sandviken, Sweden.

*Zeron 100 is a trademark of Weir Materials and Foundries, Manchester, UK.

D. *Comparison to ThermoCalc Calculations*

The commercially available thermodynamic software package, ThermoCalc,[7,8] was used to calculate stable and metastable phase equilibria for the cast alloys studied. The most recent Fe database, TCFE3, was used. Figure 13 shows the predicted equilibrium mole fraction of phases *vs* temperature in the CD3MN and CD3MWCuN alloys. According to this figure, the amount of sigma formed is at least a factor of 2 greater than the amount of chi in terms of mole fraction. It was possible to calculate the equilibrium amount (*i.e.*, volume percent) of sigma using ThermoCalc. However, the same could not be done for chi because the molar volume of chi is not present in the database used.[27] The volume of chi at 800 °C was estimated using the ThermoCalc results for total molar volume, and calculating the molar volume of chi using the crystal structure data in Table I. The results, presented in Table VIII, show that the volume fraction of sigma is always significantly greater than chi, as suggested in Figure 13. The experimental results show good agreement with calculations.

It is also seen from Figure 13 that the maximum temperature for the formation of sigma phase is predicted to be about 880 °C and 970 °C for CD3MN and CD3MWCuN, respectively. Experimentally, the maximum temperatures were found to be slightly above 900 °C for CD3MN (Figure 5) and around 1000 °C for CD3MWCuN (Figure 9). This discrepancy is not attributed to the formation of chi because, experimentally, chi usually forms at lower temperature than sigma.[28] However, further optimization of thermodynamic

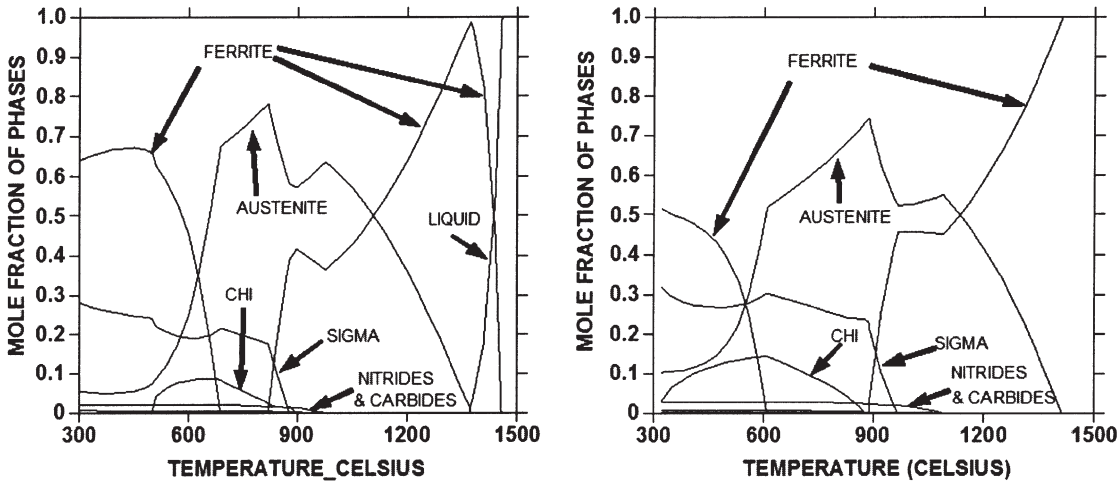

Fig. 13—ThermoCalc calculation plotted using TCFE3 database for nominal compositions of CD3MN in (*a*) mole fraction of phases *vs* temperature and CD3MWCuN in (*b*) mole fraction of phases *vs* temperature.

Table VIII. Summary of Experimental and Calculated Phase Volume Percent at 800 °C Using Nominal Compositions of CD3MN and CD3MWCuN; Maximum Sigma Phase Formation Temperature is Also Shown

	CD3MN		CD3MWCuN	
	Max. Temp., °C	Vol Pct at 800 °C	Max. Temp., °C	Vol Pct at 800 °C
Experiment				
σ including χ	~920	~11.75 ± 2.68	~1000	~28.48 ± 2.88
Predicted by ThermoCalc				
σ phase	~880	~9.80	~970	~18.0
Calculated from Table I using $V_m^{\chi} = 7.37 \times 10^{-6}$ m^3/mole				
χ phase		6.18		9.00

variables for accurate prediction for such systems is apparently needed.

V. CONCLUSIONS

1. Two types of cast duplex stainless steels, CD3MN and CD3MWCuN, were studied. The kinetics and extent of sigma formation were much greater in CD3MWCuN. For both steels, the sigma formation takes place in the approximate temperature range 700 °C to 1000 °C, with the kinetics of sigma formation being fastest at about 850 °C.
2. The faster kinetics of sigma formation in CD3MWCuN is attributed to the relatively high Cr and Mo contents in this alloy, which in turn provide for a higher driving force for sigma nucleation.
3. Comparison of TTT diagrams of cast DSS to wrought counterpart DSS indicates that the sigma-phase transformation is slower in the cast alloys than in the counterpart wrought alloys. This is believed to be due primarily to the difference in nominal compositions and microstructures between wrought and cast alloys.
4. Calculation of phase equilibria using ThermoCalc and the TCFE3 database does not completely agree with the experimental results. Further optimization of thermodynamic variables using such a database is still required for cast DSS systems.

ACKNOWLEDGMENTS

This work was funded by the United States Department of Energy (USDOE) through a subcontract with the University of Alabama, and was in collaboration with the Steel Founders' Society of America (SFSA) and their members. The authors are especially grateful to Eric Johnson and the John Deere Technology Center (Moline, IL), Keokuk Steel Castings (Keokuk, IA), and Stainless Foundry and Engineering, Inc. (Milwaukee, WI), for technical assistance, samples, and access to their facilities.

REFERENCES

1. Special Report No. 31, M. Blair, ed., Steel Founders' Society of America, Crystal Lake, IL, 2001, pp. 1-52.
2. *Duplex Stainless Steels: Microstructure, Properties and Applications*, R.N. Gunn, ed., Abington Publishing, Cambridge, United Kingdom, 1997.
3. *ASM Specialty Handbook: Stainless Steels*, J.R. Davis, ed., ASM INTERNATIONAL, Materials Park, OH, 1994.
4. J. Charles: *Proc. Conf. on Duplex Stainless Steels'91*, Les Editions de Physique, Beaune, France, 1991, vol. 1, pp. 3-48.
5. E.M. Johnson, Y.-J. Kim, L.S. Chumbley, and B. Gleeson: *Scripta Mater.*, 2004, vol. 50, pp. 1351-54.
6. J.W. Christian: *The Theory of Transformations in Metals and Alloys*, 2nd ed., Pergamon, New York, NY, 1975.
7. N. Saunders and A.P. Miodownik: *CALPHAD (Calculation of Phase Diagrams), a Comprehensive Guide. Pergamon Materials Series*, Elsevier, Oxford, United Kingdom, 1998, vol. 1.

8. J.-O. Andersson, T. Helander, L. Hoglund, P. Shi, and B. Sundman: *CALPHAD*, 2002, vol. 26, pp. 273-312.
9. J.-O. Nilsson, P. Kangas, T. Karlsson, and Q. Wilson: *Metall. Mater. Trans. A*, 2000, vol. 31A, pp. 35-45.
10. Y.H. Lee, K.T. Kim, Y.D. Lee, and K.Y. Kim: *Mater. Sci. Technol.*, 1998, vol. 14, pp. 757-64.
11. *Proc. Conf. Duplex Stainless Steels'83*, R.A. Lula, ed., ASM INTERNATIONAL, Materials Park, OH, 1983, vol. 1, pp. 693-756.
12. B. Josefsson, J.-O. Nilsson, and A. Wilson: in *Duplex Stainless Steels'91*, J. Charles and S. Bernhardsson, eds., Les Editions de Physique, Beaune, France, 1991, vol. 1, pp. 67-75.
13. X.G. Wang, D. Dumortier, and Y. Riquier: in *Duplex Stainless Steels'91*, J. Charles and S. Bernhardsson, eds., Les Editions de Physique, Beaune, France, 1991, vol. 1, pp. 127-34.
14. K.M. Lee, H.S. Cho, and D.C. Choi: *J. Alloys Compounds*, 1999, vol. 285, pp. 156-61.
15. T.H. Chen and J.R. Yang: *Mater. Sci. Eng. A*, 2002, vol. A311, pp. 28-41.
16. Y.S. Sato and H. Kokawa: *Scripta Mater.*, 1999, vol. 40, pp. 659-63.
17. Y. Maehara, M. Koike, N. Fujino, and T. Kunitake: *Trans. Iron Steel Inst. Jpn.*, 1983, vol. 23, pp. 240-46.
18. A. Gregori and J.-O. Nilsson: *Metall. Trans. A*, 2002, vol. 33A, pp. 1009-18.
19. M. Ceylan, V. Kuzucu, M. Aksoy, I. Aksoy, M. Kaplan, and M.M. Yildirim: *J. Mater. Proc. Technol.*, 1997, vol. 69, pp. 238-46.
20. V. Kuzucu, M. Ceylan, M. Aksoy, I. Aksoy, and M. Kaplan: *J. Mater. Proc. Technol.*, 1997, vol. 69, pp. 247-56.
21. E.L. Brown, T.A. Whipple, and G. Krauss: in *Duplex Stainless Steels '91*, J. Charles and S. Bernhardsson, eds., Les Editions de Physique, Beaune, France, 1991, vol. 1, pp. 665-91.
22. J.A. Jimenez, M. Carsi, O. Ruano, and F. Penalba: *J. Mater. Sci.*, 2000, vol. 35, pp. 907-15.
23. J. Li, T. Wu, and Y. Riquier: *Mater. Sci. Eng. A*, 1994, vol. A174, pp. 149-56.
24. S. Bugat, J. Besson, A.F. Gourgues, F. N'Guyen, and A. Pineau: *Mater. Sci. Eng. A*, 2001, vol. A317, pp. 32-6.
25. T.H. Chen, K.L. Weng, and J.R. Yang: *Mater. Sci. Eng. A*, 2002, vol. A338, pp. 259-70.
26. T. Kuroda, K. Nakade, and K. Ikeuchi: *Welding World*, 2000, vol. 44, pp. 17-22.
27. B.J. Lee: Pohang University of Science and Technology, Pohang, Korea, private communication, 2004.
28. X. Li, A.P. Miodownik, and N. Saunders: *Mater. Sci. Technol.*, vol. 18, pp. 861-68.